Effect of chemical doping on the ferroelectric neutral-ionic phase transition in tetrathiafulvalene-*p*-chloranil (TTF-QCl_4)

S. Horiuchi, R. Kumai, and Y. Okimoto
Joint Research Center for Atom Technology (JRCAT), Tsukuba 305-0046, Japan

Y. Tokura
Joint Research Center for Atom Technology (JRCAT), Tsukuba 305-0046, Japan
and Department of Applied Physics, The University of Tokyo, Tokyo 113-0033, Japan
(Received 16 October 1998)

Effects of molecular substitution on the neutral-ionic (NI) phase transition have been investigated for tetrathiafulvalene (TTF)-*p*-chloranil (QCl_4) complex doped with tetraselenafulvalene (TSF) or trichloro-*p*-benzoquinone (QCl_3) molecules. Except for the fully substituted compound TTF-QCl_3 of minor structural modifications, x-ray-diffraction measurements confirm the isostructurality over a wide compositional range as well as smooth change in the lattice constants by molecular replacement. With increasing TSF concentration, the peak in the dielectric constant corresponding to the ferroelectric NI transition smoothly shifts toward zero temperature due to the lattice expansion. Around the critical concentration are found some characteristics of quantum ferro(para)electricity. Although the increment of QCl_3 concentration also lowers the peak temperature of the dielectric constant, the dielectric anomalies reveal glasslike frequency dependence. We attributed the glasslike behavior to the strong ''pinning-impurity'' effect of QCl_3 which yields binary-phase separation into ferroelectric (ionic) and paraelectric (neutral) regions. [S0163-1829(99)03617-6]

I. INTRODUCTION

Organic charge-transfer (CT) complexes have provided a wealth of attractive phenomena besides the conducting and superconducting properties observed for a class with segregated molecular assemblies (columns or layers) of a donor (D) and an acceptor (A). Also for the semiconducting compounds with alternately stacked D and A molecules (mixed stack), low-dimensional nature in electronic and magnetic properties produces some characteristic structural phase transitions and related unusual phenomena.

The 1:1 mixed stack CT complexes are classified into either quasineutral (N) or quasi-ionic (I) according to their electronic ground states. For the ionic state, the D^+ and A^- molecules with $S=\frac{1}{2}$ spins are usually coupled with antiferromagnetic superexchange interactions and their regular stacks are unstable against the dimeric distortion producing singlet D^+A^- pair at low temperature. This phase transition, which is widely observed for the ionic crystals, is similar to the spin-Peierls transition. Furthermore, such a strongly electron (spin)-lattice-coupled system has been proved to accompany the one-dimensional ferroelectricity of the DA lattice, although merely a very few studies have been so far reported on their dielectric properties.[1]

Some neutral mixed stack compounds also undergo an analogous dimerization related structural transition in the course of the neutral-ionic (NI) phase transition. The NI phase transition, which can be driven by application of pressure[2] or much more rarely by lowering temperature at ambient pressure, accompanies a distinct change in molecular valence, namely the transformation between nonmagnetic phases of regular neutral stacks and of dimerized ionic ones. The temperature induced NI transition was extensively studied on tetrathiafulvalene (TTF)-*p*-chloranil (QCl_4) complex as the first and prototypical example[3] until the recent discovery of three additional compounds.[4–6] In TTF-QCl_4, the degree of CT (ρ) determined by optical spectroscopies abruptly increases from 0.3 to 0.7 at $T_c=81$ K on lowering temperature.[7,8] The simultaneous dimeric distortion of molecular stacks[7,8] has been proved to be a ferroelectric-type by recent structural[9] and dielectric studies.[10] The low-frequency infrared absorption spectra proved the existence of a soft phonon mode, indicating a displacive nature of this phase transition.[11] Ferroelectric molecular arrangement is also observed for the 4,4′-dimethyltetrathiafulvalene-QCl_4 complex in the ionic phase at low temperature.[12] The NI transition can be thus regarded as a unique phenomenon showing such ferroelectricity as realized by both the valence and spin-Peierls-like instabilities. Incidentally, another anomalous dielectric response emerges in the neutral phase of TTF-QCl_4 due to the dynamics of the charged defects perhaps arising from the thermally excited ionic domains.[10]

According to the recently proposed P-T phase diagram,[13] application of pressure up of 1 GPa continuously shifts the transition temperature at 81 K up to room temperature. At the same time, the thermally excited NI domain walls having very low excitation energy near the critical temperature[14] increasingly mix both neutral and ionic molecular domains, reducing the discontinuity of the phase transitions.[15,16]

Our previous work on the dielectric properties demonstrated the possibility that the NI transition temperature can be continuously suppressed down to zero temperature mainly by ''chemical pressure'' effect as the mixed crystals with the selenium analog of TTF, tetraselenafulvalene (TSF) molecules.[17] Since the electron donating or accepting ability of the component molecule critically affects the valence in-

stability, its tuning can be expected as a different approach to controling the NI transition temperature. According to the previous work by Tokura *et al.*, replacement by trichloro-*p*-benzoquinone (QCl_3) molecule with weaker electron accepting ability serves to lower the NI transition temperature of TTF-QCl_4.[18] At the same time, the neutral molecular domains locally created around these impurity molecules in the ionic lattice lead to the formation of the inhomogeneous structure. One may expect the different dielectric properties between these two alloy systems, and the subsequent sections describe observations of this expectation.

II. EXPERIMENT

TTF, TSF, and QCl_4 were purchased, and QCl_3 was synthesized according to the literature.[19] All these donors and acceptors were purified by the repeated recrystallization and sublimation processes, and identified by elemental analyses. The needle-shaped single crystals of pure TTF-QCl_4 and alloyed $TTF_{1-x}TSF_x$-QCl_4 and TTF-$(QCl_4)_{1-y}(QCl_3)_y$ were grown in slowly cooled acetonitrile solution of the components. The dry acetonitrile was distilled under argon atmosphere before use. The fractions of TSF (x) and QCl_3 (y) in the alloyed samples were determined by the elemental analyses or by the lattice parameters a for TSF and c for QCl_3-doped samples. The attempt to incorporate TSF molecules beyond the composition of $x=0.5$ was prevented by the formation of undesired microcrystals of a distinct phase, which decompose in air seemingly by losing the solvent molecules. The substitution by QCl_3 molecules beyond $y=0.6$ resulted in the formation of very fine needles which are unsuitable for x-ray diffraction and dielectric measurements on a single crystal. Instead, cosublimation of the component materials gave the crystals of end material TTF-QCl_3 ($y=1$) as thick platelets with two crystallographic modifications (monoclinic and triclinic form).

All the x-ray-diffraction measurements were performed at room temperature using the automatic four-circle Rigaku AFC7R diffractometer with graphite monochromated MoKα radiation. The lattice parameters of neat and doped TTF-QCl_4 crystals were determined by using 25 reflections with $25° \leqslant 2\theta \leqslant 30°$. For two modifications of TTF-QCl_3, crystal data and experimental details are listed in Table I, and the atomic parameters are listed in Tables II and III. All the calculations were performed using the teXsan crystallographic software package of the Molecular Structure Corporation.[20]

The dielectric constant was measured in a frequency range of 0.3–100 kHz with an LCR meter (HP 4284A) using a four-probe configuration at several fixed frequencies. The ac electric field was applied parallel to the *DA* stack onto the crystal end sections, which were painted by a gold paste as electrodes after cutting into short pieces from needle-shaped crystals.

III. CRYSTAL STRUCTURES OF NEAT AND ALLOYED CRYSTALS

Both the $TTF_{1-x}TSF_x$-QCl_4 and TTF-$(QCl_4)_{1-y}(QCl_3)_y$ crystals gave the isostructural monoclinic unit cell, the parameters of which vary linearly with the fractions x and y as drawn by solid and dotted lines, respectively, in Fig. 1. The observation of anisotropic lattice expansion/shrinkage can be consistently elucidated by the intermolecular interactions of the substituted atoms for the both alloy systems as discussed below. The formation of isostructural TTF-$(QCl_4)_{1-y}(QCl_3)_y$ crystals is consistent with the previous observations by powder x-ray measurements.[18] The crystal structure determinations for $x=0.48$ and $y=0.55$ samples confirm that the overall crystal structures with the space group $P2_1/n$ are preserved on the substitution by TSF or QCl_3 molecules. Therefore the crystal structure of TTF-QCl_4[21] illustrated in Fig. 2 is also representative of that for these alloyed crystals.

TABLE I. Crystal data and experimental details for TTF-QCl_3 crystals.

	Monoclinic form	Triclinic form
Chemical formula	$C_{12}H_5Cl_3O_2S_4$	
Formula weight	415.81	
a/Å	7.643(4)	7.643(3)
b/Å	27.706(7)	28.007(8)
c/Å	7.344(8)	7.355(6)
α/°		93.41(4)
β/°	90.34(7)	90.58(4)
γ/°		97.48(3)
V/Å^3	1555(1)	1557(1)
Space group	$P2_1$	$P\bar{1}$
d_{calc}/g cm^{-3}	1.78	1.77
Z	4	4
Dimensions, mm	0.30×0.18×0.10	0.25×0.20×0.07
$2\theta_{max}$/°	55	55
Scan technique	2θ-ω	2θ-ω
Total reflections	3923	7701
Reflections used [$3\sigma(I)<I$]	2523	3556
R, R_w	0.039, 0.036	0.048, 0.044
Weighting scheme	$1/\sigma^2$	$1/\sigma^2$

The determination of lattice parameters correlating well with the composition manifests itself as an available tool to estimate unknown doping levels. In the present work, the most changeable parameters a and c was employed for determination of x and y, respectively, except for the samples plotted in Fig. 1 based on elemental analyses. The experimental error in these lattice parameters corresponds to an accuracy of ± 0.01 and ± 0.02 in x and y, respectively.

The replacement of TTF by TSF molecules enlarges only the parameters a and b without appreciable change in the c-axis parameter. Along the former two directions, the sulfur atoms are connected with neighboring QCl_4 molecules by S-Cl and S-C interactions, the distance of which is comparable or shorter than the sum of the van der Waals radii for $x=0$ crystal. On the other hand, there are no corresponding interactions along the c direction. The substitution of sulfur (in TTF) by selenium (in TSF) enlarges these atomic distance, expanding the lattice along a and b directions. The averaged distance between the molecules along the stack increases from 3.39 Å for $x=0$ to 3.45 Å for an $x=0.48$ crystal.

For the TTF-$(QCl_4)_{1-y}(QCl_3)_y$ compounds, the present work determined the crystal structure as well as the lattice

TABLE II. Atomic coordinates and equivalent isotropic thermal parameters of monoclinic TTF-QCl_3.

Atom	x	y	z	B_{eq} [a]
S(1)	0.8923(2)	0.3320(9)	−0.0629(2)	3.64(4)
S(2)	1.1023(2)	0.2469(9)	−0.1557(2)	3.40(4)
S(3)	0.5769(2)	0.2619(9)	0.0721(2)	3.22(4)
S(4)	0.7876(2)	0.1768(9)	−0.0266(2)	3.20(4)
C(5)	0.9072(7)	0.2688(9)	−0.0687(8)	2.66(10)
C(6)	1.0969(9)	0.3416(9)	−0.1552(9)	4.0(1)
C(7)	1.1919(8)	0.3035(9)	−0.1951(9)	4.0(1)
C(8)	0.7752(7)	0.2390(9)	−0.0142(8)	2.82(10)
C(9)	0.4901(8)	0.2053(9)	0.1127(8)	3.3(1)
C(10)	0.5815(8)	0.1670(9)	0.0691(8)	3.6(1)
S(15)	0.3034(2)	0.0732(9)	0.2924(2)	3.28(4)
S(16)	0.0951(2)	−0.0125(9)	0.1916(2)	3.20(4)
S(17)	0.6210(2)	0.0036(9)	0.4228(2)	3.08(3)
S(18)	0.4081(2)	−0.0823(8)	0.3333(2)	2.94(3)
C(19)	0.2943(7)	0.0091(9)	0.2792(8)	2.65(10)
C(20)	0.0975(8)	0.0817(9)	0.1949(8)	3.6(1)
C(21)	0.0069(8)	0.0433(9)	0.1501(8)	3.5(1)
C(22)	0.4241(7)	−0.0193(9)	0.3364(7)	2.46(9)
C(23)	0.7081(7)	−0.0529(9)	0.4697(8)	3.2(1)
C(24)	0.6107(8)	−0.0912(9)	0.4324(9)	3.5(1)
C(29)	0.6903(7)	0.2839(9)	0.5160(8)	2.7(1)
C(30)	0.6786(7)	0.2307(9)	0.5194(8)	2.5(1)
C(31)	0.8130(7)	0.2013(9)	0.4669(8)	2.69(10)
C(32)	0.9777(8)	0.2230(9)	0.3929(8)	2.8(1)
C(33)	0.9846(7)	0.2765(9)	0.3911(8)	2.8(1)
C(34)	0.8577(7)	0.3051(9)	0.4416(8)	3.0(1)
O(35)	0.5738(5)	0.3094(9)	0.5724(6)	3.8(1)
Cl(36)	0.4866(2)	0.2072(9)	0.5942(2)	3.67(4)
Cl(37)	0.8047(2)	0.1408(9)	0.4769(3)	4.37(4)
O(38)	1.0932(5)	0.1980(9)	0.3397(6)	4.2(1)
Cl(39)	1.1791(2)	0.3006(8)	0.3141(2)	4.20(4)
C(41)	0.2160(8)	−0.0382(9)	0.7491(8)	3.0(1)
C(42)	0.1987(8)	0.0151(9)	0.7445(8)	2.9(1)
C(43)	0.3271(8)	0.0450(9)	0.7969(7)	2.9(1)
C(44)	0.4953(8)	0.0259(9)	0.8723(8)	3.0(1)
C(45)	0.5089(8)	−0.0275(9)	0.8746(8)	3.2(1)
C(46)	0.3838(8)	−0.0573(9)	0.8219(8)	3.2(1)
O(47)	0.1008(5)	−0.0650(9)	0.6948(6)	4.2(1)
Cl(48)	0.0014(2)	0.0369(8)	0.6676(2)	4.12(4)
Cl(49)	0.3058(3)	0.1053(9)	0.7872(3)	3.69(6)
O(50)	0.6073(5)	0.0527(9)	0.9275(6)	4.3(1)
Cl(51)	0.7076(2)	−0.0491(9)	0.9509(2)	4.83(5)
Cl(52)	0.4282(6)	−0.1159(9)	0.8243(7)	3.6(1)

[a] $B_{eq}=\frac{8}{3}\pi^2[U_{11}(aa^*)^2+U_{22}(bb^*)^2+U_{33}(cc^*)^2+2U_{12}aa^*bb^*\times\cos\gamma+2U_{13}aa^*cc^*\cos\beta+2U_{23}bb^*cc^*\cos\alpha]$,where U_{ij} are temperature factors given in the form $\exp[-2\pi^2(U_{11}h^2a^{*2}+U_{22}k^2b^{*2}+U_{33}l^2c^{*2}+2U_{12}hka^*b^*+2U_{13}hla^*c^*+2U_{23}klb^*c^*)]$.

TABLE III. Atomic coordinates and equivalent isotropic thermal parameters of triclinic TTF-QCl_3.

Atom	x	y	z	B_{eq}
S(1)	0.7604(2)	−0.00763(6)	0.1127(2)	2.98(4)
S(2)	0.5847(2)	0.07774(6)	0.0463(2)	2.89(4)
C(3)	0.5709(7)	0.0143(2)	0.0336(9)	2.6(1)
C(4)	0.8737(8)	0.0490(2)	0.1766(9)	2.9(2)
C(5)	0.7914(8)	0.0870(2)	0.1470(9)	3.1(2)
S(8)	0.0178(3)	0.42242(6)	0.4914(3)	3.64(4)
S(9)	0.2662(2)	0.50724(7)	0.6197(3)	3.61(4)
C(10)	0.0587(8)	0.4857(2)	0.5261(9)	3.1(2)
C(11)	0.217(1)	0.4131(3)	0.5888(10)	4.0(2)
C(12)	0.3273(9)	0.4505(3)	0.6452(10)	3.8(2)
S(15)	0.3172(2)	0.16387(6)	0.7965(3)	3.55(4)
S(16)	0.1490(2)	0.24954(7)	0.9083(3)	3.46(4)
S(17)	0.6662(2)	0.23382(6)	0.6783(2)	3.13(4)
S(18)	0.4970(2)	0.31908(6)	0.7954(2)	3.17(4)
C(19)	0.3356(8)	0.2266(2)	0.8168(8)	2.6(1)
C(20)	0.1063(10)	0.1554(3)	0.8834(10)	4.0(2)
C(21)	0.0296(9)	0.1936(3)	0.9354(10)	3.8(2)
C(22)	0.4783(8)	0.2562(2)	0.7703(8)	2.6(1)
C(23)	0.7830(8)	0.2908(2)	0.6514(9)	3.2(2)
C(24)	0.7070(9)	0.3287(3)	0.7020(9)	3.5(2)
C(29)	0.3765(9)	0.0324(2)	0.4468(9)	3.0(2)
C(30)	0.5550(8)	0.0510(2)	0.5255(9)	2.9(2)
C(31)	0.6663(8)	0.0207(2)	0.5726(8)	2.8(2)
O(32)	0.2761(6)	0.0595(2)	0.3998(7)	4.3(1)
Cl(33)	0.6183(5)	0.1105(1)	0.5446(5)	3.31(8)
Cl(34)	0.8745(2)	0.04173(7)	0.6537(3)	4.46(5)
C(35)	0.5422(8)	0.2118(2)	0.2298(8)	2.6(1)
C(36)	0.5791(8)	0.2658(2)	0.2378(8)	2.5(1)
C(37)	0.4592(8)	0.2937(2)	0.2949(8)	2.9(2)
C(38)	0.2853(8)	0.2728(2)	0.3615(9)	2.9(2)
C(39)	0.2528(8)	0.2192(2)	0.3531(8)	2.7(1)
C(40)	0.3717(8)	0.1908(2)	0.2976(9)	2.9(2)
O(41)	0.6482(6)	0.1869(2)	0.1662(6)	3.6(1)
Cl(42)	0.7839(2)	0.28903(6)	0.1681(3)	3.65(4)
Cl(43)	0.4968(3)	0.35508(6)	0.3014(3)	4.27(5)
O(44)	0.1803(6)	0.2979(2)	0.4237(7)	4.2(1)
Cl(45)	0.0475(2)	0.19484(7)	0.4245(3)	4.18(5)
C(47)	0.1553(10)	0.5321(2)	0.0695(9)	3.3(2)
C(48)	0.1469(10)	0.4788(3)	0.0592(9)	3.4(2)
C(49)	0.0039(10)	0.4492(2)	0.0001(9)	3.4(2)
O(50)	0.2818(7)	0.5579(2)	0.1325(7)	4.6(1)
Cl(51)	0.3330(3)	0.45660(7)	0.1295(3)	4.89(5)
Cl(52)	0.0087(5)	0.3894(1)	−0.0028(5)	3.78(9)

parameters of improved accuracy compared to the previous study[18] on the powder. QCl_3-doping results in large and small shrink along the a and c axes, respectively, while the b parameter is almost independent of y. The noncentrosymmetric QCl_3 molecules, which are still located on the center of inversion in the crystal, inevitably possess the orientational disorder with respect to the chlorine sites. The chlorine atoms occupy two kinds of crystallographically independent sites, only one of which is involved in the substitution by hydrogen atoms (filled circles in Fig. 2) according to the population analyses for the $y=0.55$ crystal. These disordered chlorine sites participate in the intermolecular Cl··Cl interaction running along the c direction (solid lines in Fig. 2) with the atomic distance (3.51 Å for $y=0$) comparable to the sum of van der Waals radii. The substantial contraction of the c axis can be well explained by the shortened averaged

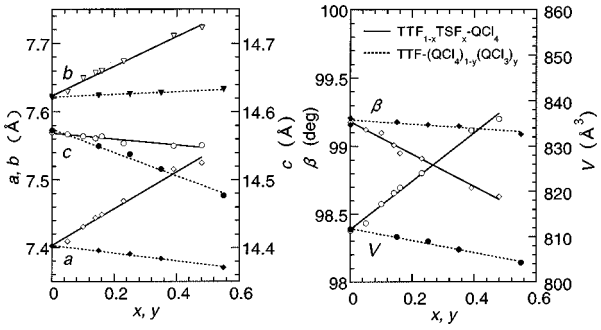

FIG. 1. Lattice parameters for monoclinic crystals of $TTF_{1-x}TSF_x$-QCl_4 and TTF-$(QCl_4)_{1-y}(QCl_3)_y$ with various x or y. Solid and dotted lines represent the least-squares fit to the linear dependencies on x or y.

C··Cl (or H) distance on the substitution by smaller hydrogen atoms.

For the end material TTF-QCl_3 ($y=1$), the previously studied x-ray powder pattern was found to resemble those of the alloyed crystals, but did not assure whether the crystal structure is the same.[18] The present work has clarified the crystal structures with finding of two structural modifications, as is illustrated in Fig. 3 for both monoclinic and triclinic phases of TTF-QCl_3 crystals. Both crystal phases include the *DA* columns of completely ordered QCl_3 molecules, which alternate along the *b* direction with those containing disordered chlorine sites of two orientations marked by filled circles in the figure. The molecular arrangement parallel to the *ac* plane for the two TTF-QCl_3 phases are essentially the same as that along the *ab* plane for the TTF-QCl_4, as is evident in the parameters *a*, *c*, and β being almost equal to the corresponding parameters *b*, *a*, and γ ($=90°$) in the TTF-QCl_4 crystal. These three crystal structures are distinguished by the interstack packing motifs along the lateral directions. In the TTF-QCl_4 crystal, a column A denoted in Fig. 2 is related to the neighboring column B by a twofold axis. The infinite repetition ABAB··· along the *c* direction is viewed as a herringbone by projecting on the stacking axis. Although this repetition unit AB is also embedded in the arrangement along the *b* direction for both TTF-QCl_3 crystal phases, it is locally broken so as to form AB|B′A′|AB|B′A′··· array for the monoclinic form and ABA|A′|ABA|A′··· array for the triclinic form. In both cases, all the hydrogen atoms in the ordered QCl_3 molecular sites are located on the terminal boundaries of AB units and responsible for structural modifications.

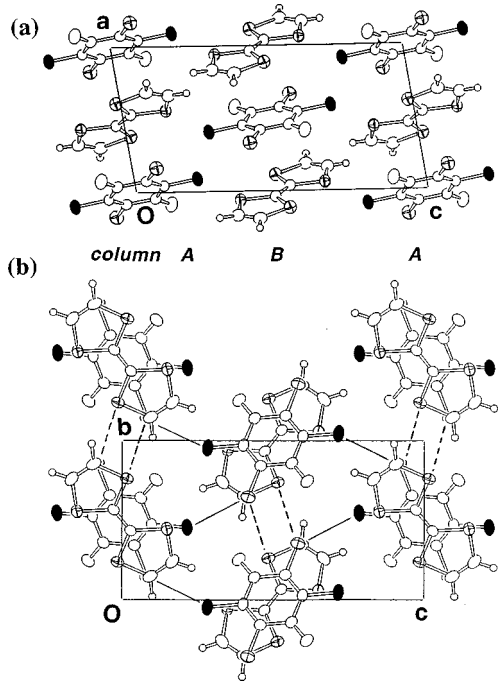

FIG. 2. Crystal structures of neat and alloyed TTF-QCl_4; (a) projected along the *b* axis and (b) along the *a* axis. Filled circles are disordered chlorine sites in QCl_3-doped crystals.

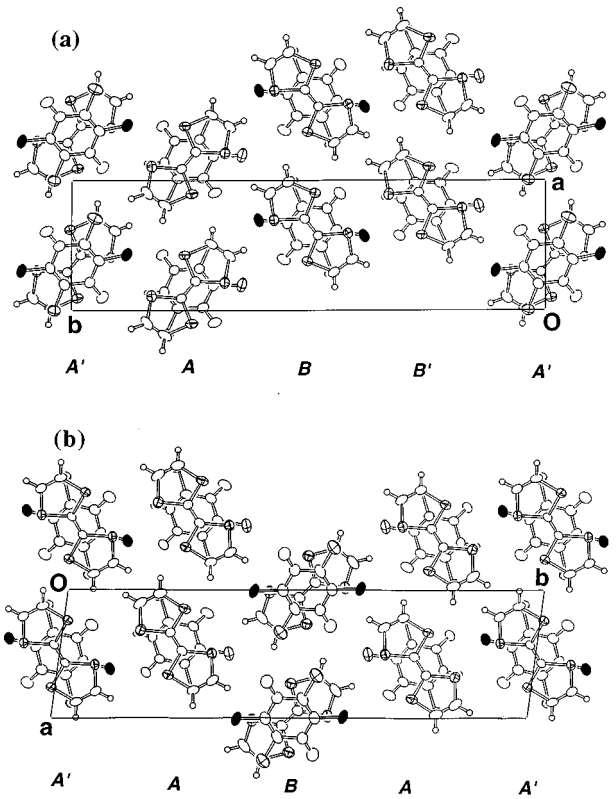

FIG. 3. Crystal structures of TTF-QCl_3 projected along the *c* axis (the stacking direction): (a) monoclinic phase and (b) triclinic phase. Filled circles are the chlorine atoms in orientational disorder.

To summarize, both donor and acceptor sites in the TTF-QCl_4 crystal are subject to isostructural substitution by TSF and QCl_3 molecules, respectively, over a wide concentration range. Furthermore, even complete substitution by QCl_3 molecules drives only slight structural modifications. The crystal structural analyses confirm that the TSF molecule is a good dopant with minimized perturbation such as the molecular shape and symmetry compared with the QCl_3 molecule, while the latter bears an additional disorder with respect to the chlorine orientation in the alloyed crystal.

IV. DIELECTRIC PROPERTIES

A. Neutral phase

The temperature dependence of the dielectric constant (ε) of nondoped and TSF-doped ($x=0.10$ and 0.48) crystals are plotted in Fig. 4 for five fixed frequencies. Below 100 K, the

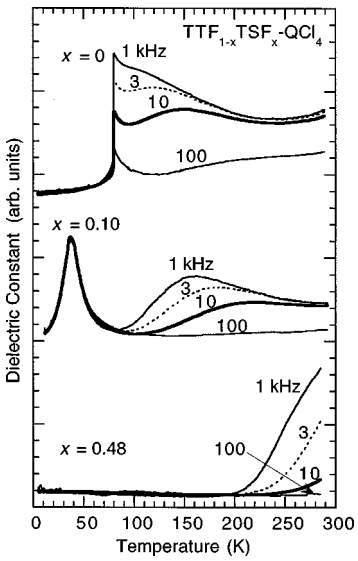

FIG. 4. Temperature dependence of the dielectric constant at different frequencies for $TTF_{1-x}TSF_x$-QCl_4 crystals with $x=0$, 0.10, and 0.49.

ε-T curve displays a sharp anomaly, which signals the ferroelectric transition for $x=0$ and 0.10 crystals. Above that temperature where the crystals are in the quasineutral state, it displays another broad peak. The peak height and temperature are significantly dependent on frequency. Similar anomalous dielectric response has already been explained by a Debye-type relaxation model for the neat TTF-QCl_4 crystals, and are interpreted as the dynamics of charged boundaries (NI domain walls) between the neutral- and excited-ionic molecular regions.[10] This frequency dispersion, which is also observed for QCl_3-doped crystals, tends to shift toward higher temperature with increasing dopant concentration. The most TSF-rich sample ($x=0.48$) displayed only a tail of this anomaly around room temperature.

The Debye model describes the frequency dependencies of the real part of dielectric function as

$$\varepsilon(\omega)=\varepsilon_\infty^+(\varepsilon_0-\varepsilon_\infty)/(1+\omega^2\tau^2), \tag{1}$$

where the ε_0 and ε_∞ are static and high-frequency dielectric constants, respectively, and τ is the relaxation time. The τ^{-1}

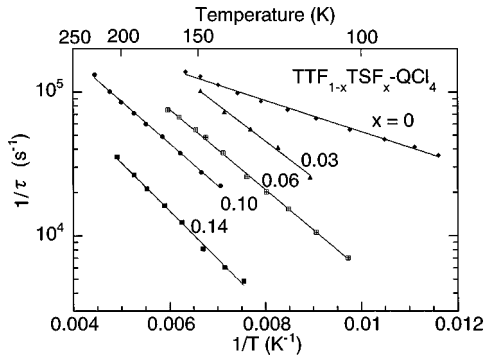

FIG. 5. Temperature dependence of the relaxation rate τ^{-1} in Debye-type dielectric response for the neutral phase of $TTF_{1-x}TSF_x$-QCl_4 with various x values.

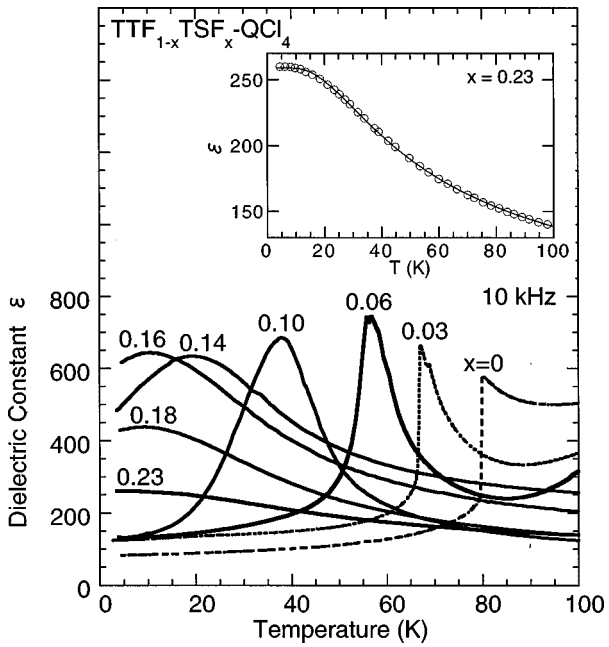

FIG. 6. Temperature dependence of the dielectric constant at 10 kHz for $TTF_{1-x}TSF_x$-QCl_4 crystals with various x values. A solid curve in the inset shows the fit to the Barrett formula [see text, Eq. (2)] for an $x=0.23$ crystal.

values obtained by fitting of the data to this relation show the temperature dependence of the thermal activation type (Fig. 5). For the pure TTF-QCl_4 crystal, this behavior was found to be parallel to that of conductivity, and the temperature-dependent mobility of the NI domain walls was proposed for their common origin.[10] With increasing dopant contents, the relaxation rate (τ^{-1}) tends to decrease at fixed temperatures responsible for the observed shift of the dielectric anomalies toward high temperature. The reduction of τ^{-1} indicates the suppression of the dynamic motion of NI domain walls by TSF doping, the effect of which is opposite to that of applied pressure. This observation can be ascribed to the stabilized neutral state going away from the NI phase boundary as will be discussed in the following sections.

The observed Debye-type relaxation, particularly the magnitude of the broad peak in the N phase, strongly depends on crystals and sometimes also on the thermal history. Also for the nondoped crystals, the observed relaxational behavior shown in Fig. 4 somewhat differs from the reported data[10] measured on the samples prepared by cosublimation. It should be noted that these two preparation methods did not show a discernible difference in the transition temperature, which is very sensitive to the chemical doping as shown later. Because the N and I phases are nearly degenerate,[14,22] we can expect that the formation of the NI domain-boundaries in the crystals are also affected by even a slight amount of impurities or defects which are inevitably introduced during the crystal growth in solution or in the course of the first-order phase transition. Therefore such extrinsic charged defects are likely responsible for the considerable variations in the dielectric response. By contrast, for the low-temperature region the ε-T curves at high frequency are little dependent on samples within the same-batch crystals.

B. Effect of chemical substitution on the phase transition

1. $TTF_{1-x}TSF_x$-QCl_4

Below 100 K, the critical dielectric anomaly is associated with the NI transition and is modified by the molecular substitution by TSF or QCl_3 in different ways. Figure 6 shows the temperature dependent dielectric constant measured at a frequency of 10 kHz for the crystals with various TSF content x. For the neat TTF-QCl_4 ($x=0$) crystal, the ε measured at high frequencies displays the Curie-Weiss-like behavior above the T_c (81–82 K) followed by a discontinuous drop with a thermal hysteresis of about 1–2 K in width. These observations are characteristic of the first-order ferroelectric phase transition.

The dielectric anomaly shifts toward lower temperature and its discontinuity and thermal hysteresis become less pronounced with increasing TSF incorporation up to $x=0.06$. The anomaly for the $x=0.06$ crystal shows up as a singular peak without discernible thermal hysteresis, suggesting that the first-order transition approaches or turns to the continuous one. For x from 0.06 to 0.18, the peak is gradually broadened and shifted toward lower temperature.

Beyond the composition of $x=0.18$, the dielectric constant becomes saturated without showing a peak structure. The saturation behavior is characteristic of the quantum paraelectricity, a phenomenon that the ferroelectric ordering is suppressed by quantum fluctuation of the lattice, as was observed, for example, in $SrTiO_3$.[23] As exemplified in the inset to Fig. 6, the observed ε-T curves can be well fitted to the Barrett formula for the quantum paraelectricity:

$$\varepsilon = A + B/[(T_1/2)\coth(T_1/2T) - T_0]. \tag{2}$$

Here, the parameter T_0 equals the Curie-Weiss temperature in a classical limit, and T_1 represents the characteristic temperature dividing the quantum-mechanical and classical regions.[24] The best fitting of the data gives the T_0 values as -28, -58, -105, and -115 K for $x=0.23$, 0.24, 0.39, and 0.48, respectively, with 40–80 K of T_1. The decrease in T_0 values with increasing x is representative of the flattening of the entire ε-T curve as a result of the suppressed dielectric response in a low-temperature region. Although the fairly high dielectric constant for these TSF-doped crystals signals the softening of a ferro(antiferro)electric phonon mode in lowering temperature, suppression of such pretransitional phenomena with increasing x indicates their ground state going away from the ferroelectric ionic one.

Figure 7(a) plots the T_c defined by the maximum position of dielectric constant against the TSF concentration. The T_c is linearly lowered on increment of TSF content up to $x=0.18$, at which the ferroelectric I phase vanishes. Despite the sensitivity of T_c to the composition, fairly small variation of T_c among different crystals from the same batch as well as the sharpness of the transition assures again the crystallization of homogeneously alloyed complexes. Around the critical concentration $x_c=0.18$, the dielectric constant at the lowest temperature (5 K) shows a steep peak as a function of x as shown in the lower panel of Fig. 7(b). The ferroelectric ordering, or equivalently the NI transition at such a low temperature is affected by quantum fluctuation, and can be termed the quantum ferroelectricity. For the quantum ferroelectricity, the ε value tends to increase near the quantum critical point displaying the relation $\varepsilon(T\rightarrow 0\ \mathrm{K}) \propto (x-x_c)^{-1}$ (Ref. 25). The $TTF_{1-x}TSF_x$-QCl_4 system displays an analogous feature, as shown by broken lines in both sides of $x_c=0.18$. It should be noted that the quantum ferroelectricity for the NI transition system accompanies the valence fluctuation or quantum coexistence of the N and I molecular domains.

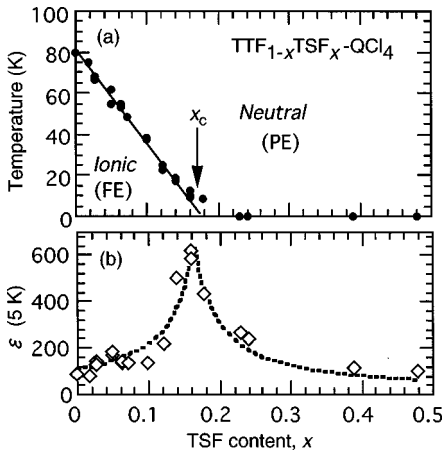

FIG. 7. TSF concentration (x) dependence of (a) the peak temperature of the dielectric constant at 10 kHz, and (b) the dielectric constant at 5 K for $TTF_{1-x}TSF_x$-QCl_4 crystals. A thick solid line represents the NI or paraelectric (PE) ferroelectric (FE) phase boundary. The dotted line is the guide to the eyes.

The expansion of the parameters a and b at $x_c=0.18$ corresponds to the effective negative pressure of -0.10 and -0.37 GPa, respectively, on the basis of the data of the pressure dependent shrinkage (0.51 and 0.12 Å/GPa, respectively[13,26]). On the other hand, the hypothetical negative critical pressure of -0.25 GPa is obtained by linear extrapolation of the P-T phase boundary with a slope of 3.1 MPa/K (Ref. 13) to zero temperature. The pressure values estimated from lattice parameters, although anisotropic, are thus comparable to this extrapolated value, confirming that the ''chemical pressure'' plays a dominant role in suppression of ferroelectric NI transition. Note that the pressure effect on the NI transition system is opposite to that for the conventional ferroelectrics of the displacive type.[27] This is because the paraelectric N phase is destabilized, due to the Madelung energy term, in a lattice compressed by application of pressure.

2. TTF-QCl_3

The weaker electron-accepting ability of QCl_3 than QCl_4 is responsible for stabilizing the neutral state of the TTF complex for the entire temperature range at ambient pressure. The critical pressure value of 1.1 GPa at room temperature for the NI transition in TTF-QCl_4 increases to 2.5 GPa in TTF-QCl_3.[16] Because of small difference in these values, we may expect that energy of the ionic ground state is still close to that of the neutral one for the TTF-QCl_3 complex. In contrast with the TTF-QCl_4, the neat TTF-QCl_3 displayed no dielectric anomalies characteristic of the ferro(antiferro)electric ordering. Below 150 K, however, the ε value tends to increase with decreasing temperature, and saturates around

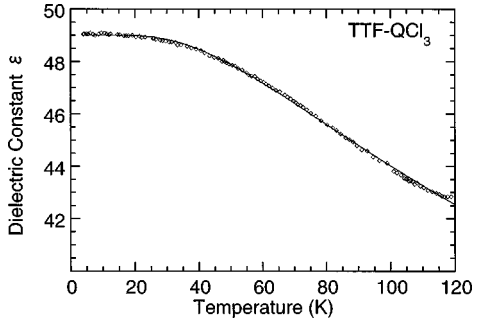

FIG. 8. Temperature dependence of the dielectric constant at 10 kHz for a TTF-QCl_3 crystal (monoclinic phase). The solid curve represents the fit to the Barrett formula for the quantum paraelectricity [see text, Eq. (2)].

the lowest temperature, deviating from the Curie-Weiss law, as shown in Fig. 8. This ε-T curve is very similar to those of some $TTF_{1-x}TSF_x$-QCl_4 crystals, the ionic state of which is removed by enriching TSF concentration. The fitting to Barrett formula yielded $T_0 = -181$ K and $T_1 = 145$ K. This dielectric response indicates that the valence instability coupled to the lattice tends to soften the ferroelectric phonon mode toward low temperature although insufficient to drive a ferroelectric ordering at ambient pressure. The observation of pretransitional phenomena confirms the energetical proximity between the N and I states also in TTF-QCl_3 crystal.

3. TTF-$(QCl_4)_{1-y}(QCl_3)_y$

Figure 9 shows the ε-T curve measured at a frequency of 10 kHz below 100 K for QCl_3-doped crystals. The partial substitution of QCl_4 by QCl_3 molecules shifts the dielectric anomaly toward lower temperature as is found for the mixed crystals with TSF. Even for the crystals with the largest y value (0.55), the maximum peak in the ε-T curve remains around 10 K. As a consequence, the alloyed samples display neither the quantum paraelectricity nor the quantum ferroelectricity for the entire QCl_3 content investigated. The peak height in the ε-T curve becomes prominent with increasing QCl_3 content up to $y = 0.15$, and rapidly suppressed by further doping. These results are in sharp contrast with the observation that the increment of TSF content smoothly shifts the dielectric peak to 0 K without changing much the maximum ε value (Fig. 6).

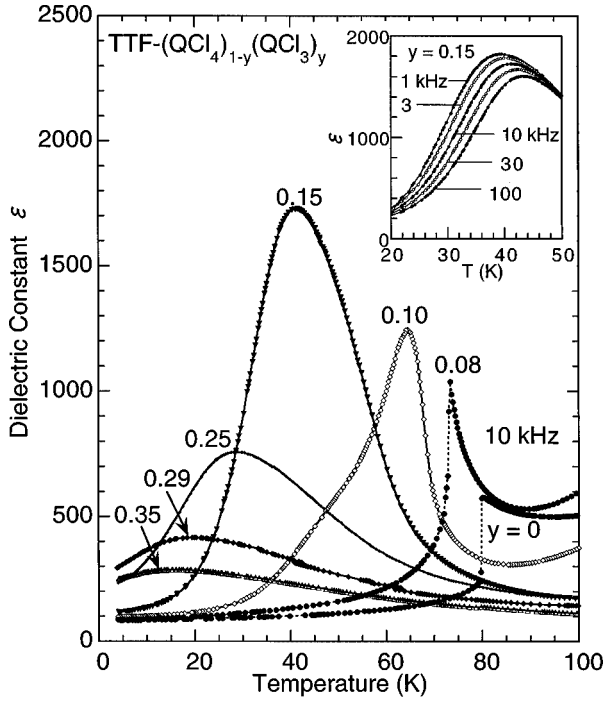

FIG. 9. Temperature dependence of the dielectric constant at 10 kHz for TTF-$(QCl_4)_{1-y}(QCl_3)_y$ crystals with various y values. The inset shows the ε-T curves at different frequencies for $y = 0.15$ crystal.

The inset to Fig. 9 shows the ε-T curves measured at different frequencies for a $y = 0.15$ crystal. Pronounced frequency dispersion appears on the low-T side of the dielectric peak. The peak shifts toward higher temperature and its amplitude decreases with increasing frequency. This frequency dispersion, which was not observed for the $TTF_{1-x}TSF_x$-QCl_4 crystals, is reminiscent of the relaxational glasses[28] and particularly pronounced for the crystals with moderate QCl_3 content ($0.15 \leqslant y \leqslant 0.25$). For $KTa_{1-x}Nb_xO_3$, which originally attracted interest as a novel example of quantum ferroelectrics, the relaxational glasslike behavior was observed under pressure and ascribed to the appearance of a local order instead of a homogeneous phase transition with long-range ordering.[29] In this compound, the Nb^{3+} ions of dilute concentration ($x \leqslant 0.02$) accommodated in quantum paraelectric $KTaO_3$ occupy off-center positions, bearing ferroelectric local order responsible for the relaxational dielectric response.

According to the previously reported optical spectra of TTF-$(QCl_4)_{1-y}(QCl_3)_y$ crystals, dopant QCl_3 molecules produce quasineutral microregions around themselves in the host TTF-QCl_4 lattice of quasi-ionic state, leading to a binary-phase separation at low temperature.[18] The temperature dependence of the respective fractions of N and I molecules turns to gradual change by QCl_3 doping. The glasslike behavior can be attributed to the dielectric response from the ferroelectric microregions isolated by the paraelectric (N) domains around QCl_3 molecules. Therefore increment of dopant concentration serves to reduce the size of ferroelectric microregion at a fixed temperature, contrary to the case of Nb^{3+} ions in $KTa_{1-x}Nb_xO_3$.[29]

In analogy to the $KTa_{1-x}Nb_xO_3$, we treat the present data by Debye-type relaxation model, which was also applied to the discussion in Sec. IV A on dielectric response for the neutral phase in TTF-QCl_4. In this model, the imaginary part of dielectric function (ε'') expressed by

$$\varepsilon''(\omega) = (\varepsilon_0 - \varepsilon_\infty)\omega\tau'/(1+\omega^2\tau'^2) \tag{3}$$

gives the maximum value at a characteristic frequency. This frequency gives a relaxation time defined as τ' ($=1/\omega$) which should be distinguished from the τ for the N phase. The peak in the ε''-T curve depends on the frequency ω via temperature dependent τ'. In the low-temperature region, contribution of the dc conductivity is completely negligible. Figure 10 plots the relaxation time τ' as a function of peak temperature for the samples with various y. The present results can be qualitatively described by a thermally activated behavior as

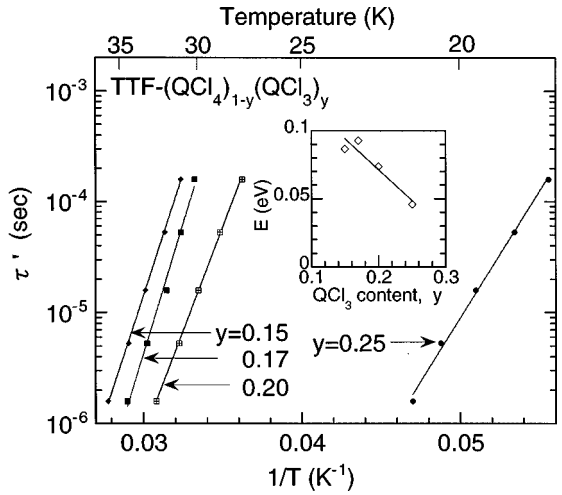

FIG. 10. Temperature dependence of the relaxation time τ' in dielectric response around the glass transition for TTF-$(QCl_4)_{1-y}(QCl_3)_y$ with various y values. The inset shows the QCl_3 concentration (y) dependence of activation energy E.

$$\tau' = \tau_0' \exp(E/k_B T). \tag{4}$$

The activation energy E obtained from the least-squares fit are 0.087, 0.093, 0.074, and 0.046 eV for $y=0.15$, 0.17, 0.20, and 0.25, respectively (see the inset to Fig. 10). In the case of $KTa_{1-x}Nb_xO_3$,[29] the E corresponds to a barrier height for hopping motion of Nb^{5+} ions among the equivalent off-center positions in the ferroelectric microregion. For the TTF-QCl_4 crystal, the mobile spin solitons, the presence of which is theoretically predicted[14] and detected by electron spin resonance measurements,[30] can convert a dipole moment of the ferroelectric region. In analogy to this, the similar mobile spin solitons or the NI domain walls at the edge of the fragmented I domains of TTF-$(QCl_4)_{1-y}(QCl_3)_y$ may be responsible for the observed relaxational dielectric response. The activation energy E is observed to decrease with QCl_3 contents or the formation of smaller N and I domains, as shown in the inset to Fig. 10. Therefore the bound motion of the charged NI domain walls[14] is the most likely origin of the observed relaxational response of these mixed crystals.

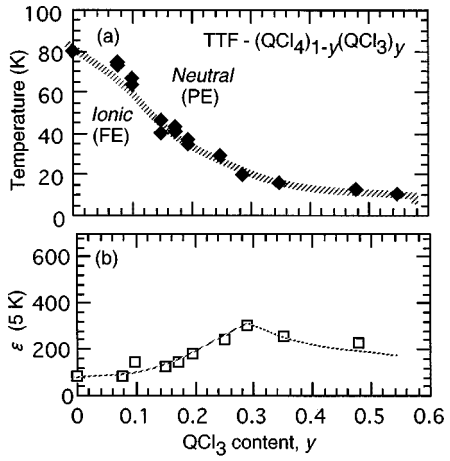

FIG. 11. QCl_3 concentration (y) dependence of (a) the peak temperature of the dielectric constant at 10 kHz, and (b) the dielectric constant at 5 K for TTF-$(QCl_4)_{1-y}(QCl_3)_y$ crystals. A shaded line as the guide to the eyes represents the glass transition representing the nominal NI phase boundary. A dotted line is the guide to the eyes.

The peak temperature of dielectric constant (T_g), which depends on the frequency, as mentioned above, is plotted against the QCl_3 content y in Fig. 11(a) with employing 10 kHz data. Whereas the T_g value agrees with the NI transition temperature for the neat TTF-QCl_4, it is representative of temperature of glass transition for doped crystals. The peak temperature T_g is smoothly lowered by increasing QCl_3 content up to $y=0.3$, although the y dependence is nonlinear unlike the x dependence of T_c for $TTF_{1-x}TSF_x$-QCl_4 system. Further increment of y results in the slower decrease of T_g, showing a saturating behavior around 10 K. Compared to the phase diagram proposed from optical spectroscopy,[18] the observed T_g value lies around the upper boundary of the binary-phase region ($\rho=0.4$ line). Therefore the appearance of a glasslike dielectric peak is seemingly associated with the initial growth of ferroelectric (ionic) molecular domains on lowering temperature.

As shown in Fig. 11(b), the dielectric constant at low temperature (5 K) is almost independent of QCl_3 concentration. In contrast with the TSF-doped crystal, dielectric response is strongly suppressed at low temperature, confirming the absence of quantum ferroelectricity for this system. As is evident from the dielectric constant, lattice of TTF-QCl_3 is much less polarizable than that of TTF-QCl_4, due to suppression of the valence instability. The replacement by QCl_3 molecules increases the area of less polarizable region, which is responsible for the reduction of the peak height with the decrease of T_g.

For the TTF-$(QCl_4)_{1-y}(QCl_3)_y$ system, the impurity effect originated from weakened electron affinity of QCl_3 overcomes the effect of lattice shrinkage, suppressing the NI transition as well as producing binary-phase separation. Such a strong ''pinning-impurity'' effect appears as a glasslike dielectric response instead of the characteristics of quantum ferroelectricity/paraelectricity. By contrast, for the $TTF_{1-x}TSF_x$-QCl_4 system, our preliminary measurements of infrared absorption spectra of powderized $x=0.10$ sample confirmed the simultaneous ionization of TSF and TTF molecules around the dielectric peak temperature ($T_c=40$ K). From a viewpoint of homogeneity of the transition, employment of ''chemical pressure'' effect by TSF doping is thus a more advantageous approach to control the NI transition temperature of alloyed system, compared with substitution by molecules of different electron donating (or accepting) ability such as QCl_3. Partial molecular substitution should more or less bring about inhomogeneity effect on the phase transition also for the $TTF_{1-x}TSF_x$-QCl_4 system, because the different molecular size may produce the microscopically inhomogeneous interplanar distance. In fact, the linear x dependence of T_c shown in Fig. 7(a) contradicts the theoretical prediction[25] that the ferroelectric transition temperature vanishes toward $x=x_c$ in proportional to $(x-x_c)^{1/2}$ by quantum effect. The rapid drop of T_c around $x=x_c$ is seemingly prevented by the impurity effect which tends to saturate the peak temperature in the low-temperature region as was more clearly observed for the TTF-$(QCl_4)_{1-y}(QCl_3)_y$ system. Concerning this problem, utilizing hydrostatic pressure as a homogeneous external parameter would be very promising

for obtaining an ideal phase diagram around the quantum critical point for the NI transition.

V. CONCLUSION

We have demonstrated a comparative study on the structural and dielectric properties of the TTF-QCl_4 crystals doped with TSF or QCl_3 molecules. The measurements of dielectric constant successfully probed the ferroelectric NI transition as a function of doping level. Furthermore, a proximity to the NI phase boundary led to the observation of pretransitional phenomena even on the samples without undergoing the transition at ambient pressure. These results manifest the usefulness of dielectric measurements also from a viewpoint of developing materials displaying a ferroelectric NI transition. Besides the continuous reduction of the transition temperature, a significant difference was found between the doping effects of TSF and QCl_3 molecules on the dielectric response. For $TTF_{1-x}TSF_x$-QCl_4 system, the volume effect plays a major role in stabilizing the neutral state, leading to the smooth decrease of T_c down to zero temperature and producing some characteristics of quantum ferro-(para)electricity. On the other hand, TTF-$(QCl_4)_{1-y}(QCl_3)_y$ is regarded as a system with strong ''pinning-impurity'' effect, since the homogeneous ferroelectric NI transition is prevented by the presence of persisting neutral region around the QCl_3 molecules. The binary-phase separation between the ionic ferroelectric and neutral paraelectric regions is regarded as the origin of the glasslike relaxation in the dielectric response.

ACKNOWLEDGMENTS

This work, partly supported by NEDO, was performed in the Joint Research Center for Atom Technology (JRCAT) under the joint research agreement between the National Institute for Advanced Interdisciplinary Research (NAIR) and the Angstrom Technology Partnership (ATP).

[1] Y. Tokura, S. Koshihara, Y. Iwasa, H. Okamoto, T. Komatsu, T. Koda, N. Iwasawa, and G. Saito, Phys. Rev. Lett. **63**, 2405 (1989).
[2] J. B. Torrance, J. E. Vazquez, J. J. Mayerle, and V. Y. Lee, Phys. Rev. Lett. **46**, 253 (1981).
[3] J. B. Torrance, A. Girlando, J. J. Mayerle, J. I. Crowley, V. Y. Lee, P. Batail, and S. J. LaPlaca, Phys. Rev. Lett. **47**, 1747 (1981).
[4] Y. Iwasa, T. Koda, Y. Tokura, A. Kobayashi, N. Iwasawa, and G. Saito, Phys. Rev. B **42**, 2374 (1990).
[5] S. Aoki, T. Nakayama, and A. Miura, Phys. Rev. B **48**, 626 (1993).
[6] S. Aoki and T. Nakayama, Phys. Rev. B **56**, R2893 (1997).
[7] A. Girlando, F. Marzola, C. Pecile, and J. B. Torrance, J. Chem. Phys. **79**, 1075 (1983).
[8] Y. Tokura, Y. Kaneko, H. Okamoto, S. Tanuma, T. Koda, T. Mitani, and G. Saito, Mol. Cryst. Liq. Cryst. **125**, 71 (1985).
[9] M. Le Cointe, M. H. Lemée-Cailleau, H. Cailleau, B. Toudic, L. Toupet, G. Heger, F. Moussa, P. Schweiss, K. H. Kraft, and N. Karl, Phys. Rev. B **51**, 3374 (1995).
[10] H. Okamoto, T. Mitani, Y. Tokura, S. Koshihara, T. Komatsu, Y. Iwasa, T. Koda, and G. Saito, Phys. Rev. B **43**, 8224 (1991).
[11] A. Moreac, A. Girard, Y. Delugeard, and Y. Marqueton, J. Phys.: Condens. Matter **8**, 3553 (1996).
[12] Y. Nogami, M. Taoda, K. Oshima, S. Aoki, T. Nakayama, and A. Miura, Synth. Met. **70**, 1219 (1995).
[13] M. H. Lemée-Cailleau, M. Le Cointe, H. Cailleau, T. Luty, F. Moussa, J. Roos, D. Brinkmann, B. Toudic, C. Ayache, and N. Karl, Phys. Rev. Lett. **79**, 1690 (1997).
[14] N. Nagaosa, J. Phys. Soc. Jpn. **55**, 2754 (1986).
[15] Y. Kaneko, S. Tanuma, Y. Tokura, T. Koda, T. Mitani, and G. Saito, Phys. Rev. B **35**, 8024 (1987).
[16] H. Okamoto, T. Koda, Y. Tokura, T. Mitani, and G. Saito, Phys. Rev. B **39**, 10 693 (1989).
[17] S. Horiuchi, R. Kumai, and Y. Tokura, J. Am. Chem. Soc. **120**, 7379 (1998).
[18] Y. Tokura, T. Koda, G. Saito, and T. Mitani, J. Phys. Soc. Jpn. **53**, 4445 (1984).
[19] Von G. Manecke and H.-J. Beyer, Makromol. Chem. **105**, 59 (1967).
[20] teXsan: Crystal Structure Analysis Package, Molecular Structure Corporation (1985 & 1992).
[21] J. J. Mayerle, J. B. Torrance, and J. I. Crowley, Acta Crystallogr., Sect. B: Struct. Crystallogr. Cryst. Chem. **35**, 2988 (1979).
[22] N. Nagaosa, Solid State Commun. **57**, 179 (1986).
[23] K. A. Müller and H. Burkard, Phys. Rev. B **19**, 3593 (1979).
[24] J. H. Barrett, Phys. Rev. **86**, 118 (1952).
[25] U. T. Höchli, H. E. Weibel, and L. A. Boatner, Phys. Rev. Lett. **39**, 1158 (1977).
[26] R. M. Metzger and J. B. Torrance, J. Am. Chem. Soc. **107**, 117 (1985).
[27] G. A. Samara, T. Sakudo, and K. Yoshimitsu, Phys. Rev. Lett. **35**, 1767 (1975).
[28] U. T. Höchli, K. Knorr, and A. Loidl, Adv. Phys. **39**, 405 (1990).
[29] G. A. Samara, Phys. Rev. Lett. **53**, 298 (1984).
[30] T. Mitani, G. Saito, Y. Tokura, and T. Koda, Phys. Rev. Lett. **53**, 842 (1984).